ELSEVIER

Fire Safety Journal 35 (2000) 77–98

FIRE SAFETY JOURNAL

www.elsevier.com/locate/firesaf

Experimental research on the critical temperature of compressed steel elements with restrained thermal elongation

J.P. Correia Rodrigues[a], I. Cabrita Neves[b,*], J.C. Valente[b]

[a]*Departamento de Engenharia Civil, Faculdade de Ciências e Tecnologia da Universidade de Coimbra, Polo II, Pinhal de Marrocos, 3030 Coimbra, Portugal*

[b]*Departamento de Engenharia Civil, Instituto Superior Técnico, Av. Rovisco Pais, 1049-001 Lisboa, Portugal*

Received 21 December 1999; received in revised form 6 April 2000; accepted 19 April 2000

Abstract

In real structures, the loading conditions of steel elements subjected to the action of a localized fire change with time, if their axial elongation is restrained. The mechanical action on these elements has a major influence on their deformation, which in turn influences the magnitude of the interaction forces between the heated elements and the cold structure. The stiffness of the structure to which compressed elements belong has a main influence on the evolution of their axial force, and subsequently on their critical temperature and on their fire resistance. This paper describes the experimental model used in the Laboratory for Structures and Strength of Materials of the Department for Civil Engineering of Instituto Superior Técnico (IST), Lisbon, Portugal, to study the critical temperature of compressed steel elements with restrained thermal elongation. A total of 168 tests on hinged bars were performed. Four different slenderness values, two eccentricities of the compression load and six levels of restraint to the axial elongation were tested. The test results and the results of a computer simulation using a finite element program show that neglecting the effect of thermal axial restraint may result in overestimation of the fire resistance of columns.

1. Introduction

A general definition for the *fire resistance* of construction elements can be as follows: *the time after which an element, when submitted to the action of a fire, ceases to*

* Corresponding author. Fax: + 351-218497650.

0379-7112/00/$ - see front matter
PII: S0379-7112(00)00018-7

fulfil the functions for which it has been designed. For the time being, the fire resistance required in most national fire safety regulations for the construction elements, does not refer to the fire that could happen with a given probability under the real conditions in a building. It is referred to a standard fire (ISO 834 [1]). Therefore, since structural elements have a load-carrying function, their standard fire resistance represents the time after which, when subjected to the standard fire, they can no longer resist the effects of the accidental load combination, according to Eurocode 1 [2]:

$$\sum \gamma_{GA} G_k + \psi_{1,1} Q_{k,1} + \sum \psi_{2,i} Q_{k,i} + \sum A_d(t), \tag{1}$$

where G_k is the characteristic values of permanent actions, $Q_{k,1}$ the characteristic value of the main variable action, $Q_{k,i}$ the characteristic value of the other variable actions, $A_d(t)$ the design values of actions from fire exposure, or indirect fire actions, γ_{GA} the partial safety factor for permanent actions in the accidental situation, and $\psi_{1,1}, \psi_{2,i}$ combination coefficients for buildings according to ENV 1991-1 [3].

The last term of this load combination represents the interaction between the heated element and the cold structure from which it is a part. The first terms represent the mechanical action on the heated element at the beginning of the fire, that is, the design effect of actions in fire situation at time $t = 0$, $E_{fi,d,t=0}$. For the analysis of the fire resistance of a single member, the Eurocodes state that "the internal forces and moments at supports and ends of members applicable at time $t = 0$, may be assumed to remain unchanged throughout the fire exposure", that is, $E_{fi,d,t} = E_{fi,d,t=0}$ [4,5–7].

Numerical simulations from earlier works [8–11] have shown that this simplification can lead in some cases to overestimation of the fire resistance of compressed elements with restrained thermal elongation. On the contrary, some attempts made in the past to take into consideration the influence of axial thermal restraint on the temperature of steel elements, like the calculation method proposed by CTICM in Ref. [12], may result in unrealistically low critical temperatures for columns, especially when those columns are a part of very stiff structures. So, it was decided to implement at IST in Lisbon, an experimental research program [9] on compressed steel bars with restrained thermal elongation. The experimental model used and the results obtained are described below.

In this work, the critical temperature of a compressed steel member with thermal elongation elastically restrained is defined as the steel temperature for which the axial force, after a thermally induced increase, decreases and reaches again the design effect of actions in fire situation at time $t = 0$. This definition is a direct consequence of the rules imposed by the Eurocodes for the structural design. In fact, it does not seem reasonable to accept the axial force acting on a column, as the effect of the load combination according to Eq. (1), when its last term $\sum A_d(t)$ has become negative. If not, one could accept at the limit an acting axial force with zero value.

2. Experimental model

The planning of the tests was made bearing in mind that the parameters to be studied should be defined and materialized as rigorously as possible, in order to

guarantee a good repeatability, under the existing constraints of a limited budget and the available equipment.

Since big furnaces to perform natural-scale tests were not available, the option was to make a set of small-scale tests on compressed steel bars with thermal elongation elastically restrained. One obvious advantage of this option is the possibility of performing a much larger number of tests at low cost. On the whole, 144 tests at high temperature were carried out.

Because it would be impossible to reproduce in small-scale some of the characteristics of the profiles used in steel construction, such as those resulting from the manufacturing process, steel bars with rectangular cross section were used. Their dimensions were chosen as a function of the slenderness values to be tested and taking into consideration the oven dimensions.

In order to guarantee constant buckling length during the heating process, hinged bars were used, having the maximum length compatible with the heating zone of the oven. For that reason all the tested bars had the same length, corresponding to a buckling length $L = 460$ mm.

In order to avoid bi-axial bending, the cylindrical supports were given the orientation of the weak axis of the cross section (Fig. 1).

Every bar had a rectangular cross-section with the greater dimension b equal to 50 mm. Therefore, the slenderness of each bar was in direct proportion to its thickness a.

In order to guarantee a constant load eccentricity in each test series, eight types of support blocks were built, one per each value of the eccentricity e of the compression load and bar thickness. These support blocks, made of stainless refractory steel, had to withstand without damage the whole testing program, supporting load levels varying from a few hundred kilos up to several tons (Figs. 1 and 2). They behaved well.

The elastic restraint to the thermal elongation of the steel bars was provided by a simply supported steel beam, named *stiffness-beam* in this paper, the stiffness of

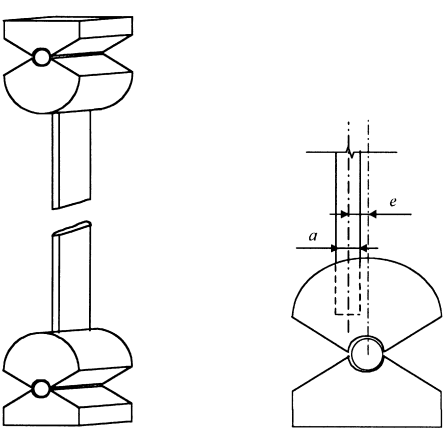

Fig. 1. Cylindrical supports.

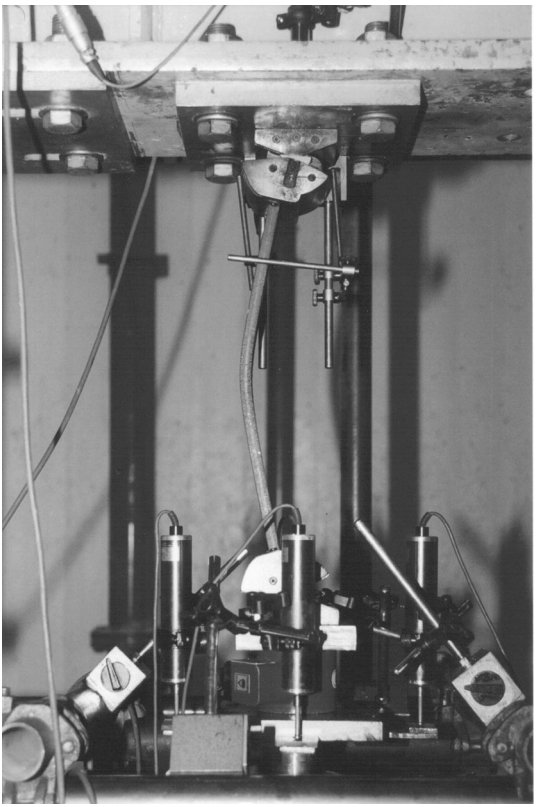

Fig. 2. Eccentric support and deflected bar after test.

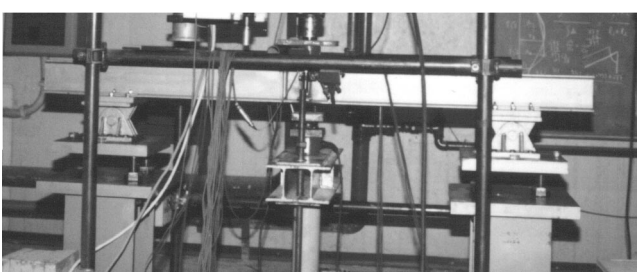

Fig. 3. Stiffness-beam with supports adjustable in height.

which was conditioned by the choice of the profile cross-section and of the span length (Figs. 3 and 4). The beam supports were adjustable in height, in order to allow for the application of an initial compression load to the hinged bar, without deformation of the beam (Fig. 3), which should behave elastically throughout the whole test.

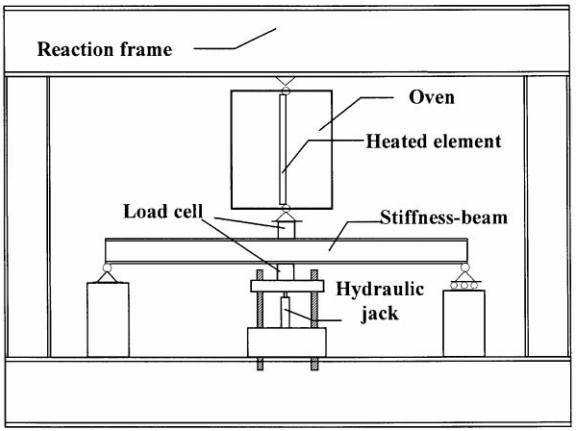

Fig. 4. The experimental model.

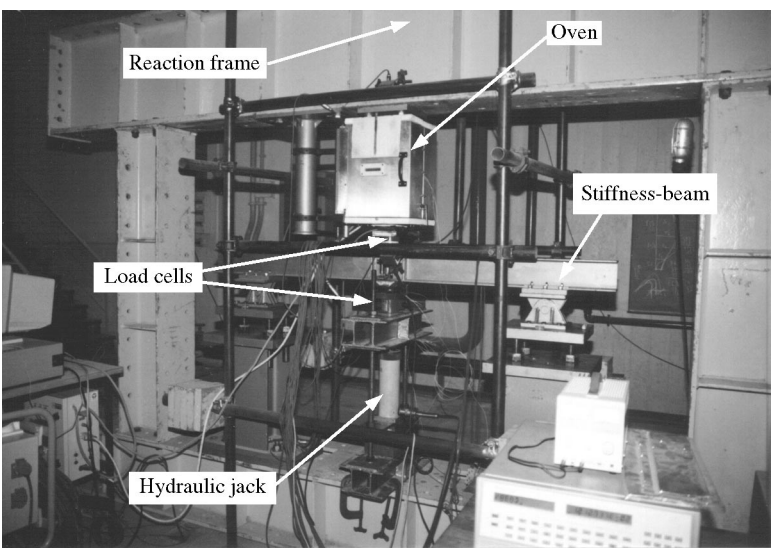

Fig. 5. General view of the experimental model.

The whole experimental model was mounted in a reaction frame with very high stiffness (Figs. 4 and 5). In order to achieve uniform heating conditions, an electric three-zone oven was used (Fig. 6). In addition to the oven temperatures in these three zones, several other variables were measured:

(1) The temperature of the steel bars at seven levels.
(2) The displacements at the bottom flange of the stiffness-beam under the lower support of the heated bar (Fig. 7).

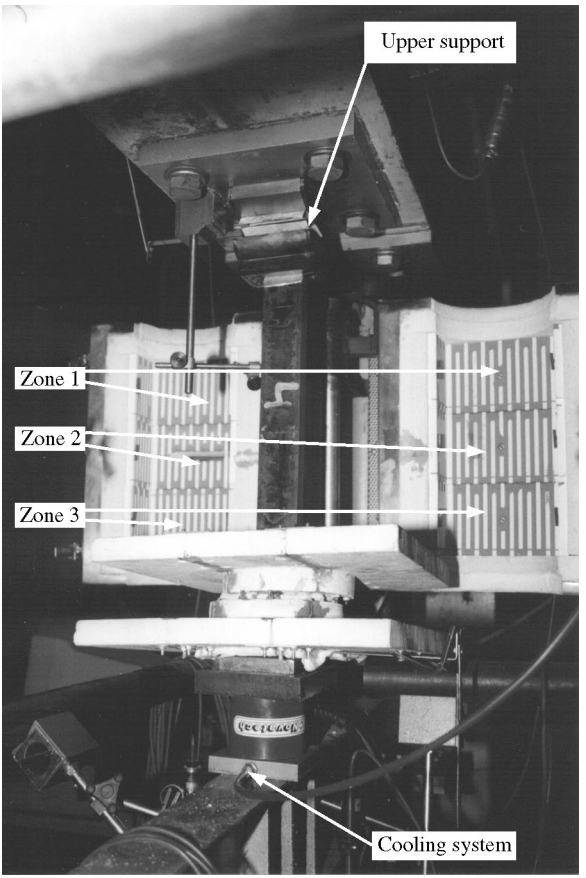

Fig. 6. Three-zone electric oven.

(3) The displacements of the reaction frame just above the upper support of the heated element, for control.

A load cell placed between the bar and the stiffness-beam (Figs. 6 and 7) measured the evolution of the restraining forces during the test. Forced air circulation through the load cell was provided to keep its temperature below the service limits imposed by the manufacturer.

At the beginning of each test, the specimen was subjected to the action of a compression load that was kept constant during the entire test. This load was applied by a hydraulic jack to the bottom flange of the stiffness-beam while keeping its supports free to move vertically (Figs. 3 and 8). Afterwards, the supports were fixed, so that the stiffness-beam could react to the elongation of the specimen during heating.

The main objective of these tests was to measure the evolution of the compression forces resulting from the elastic restraint to the thermal elongation. Therefore, special

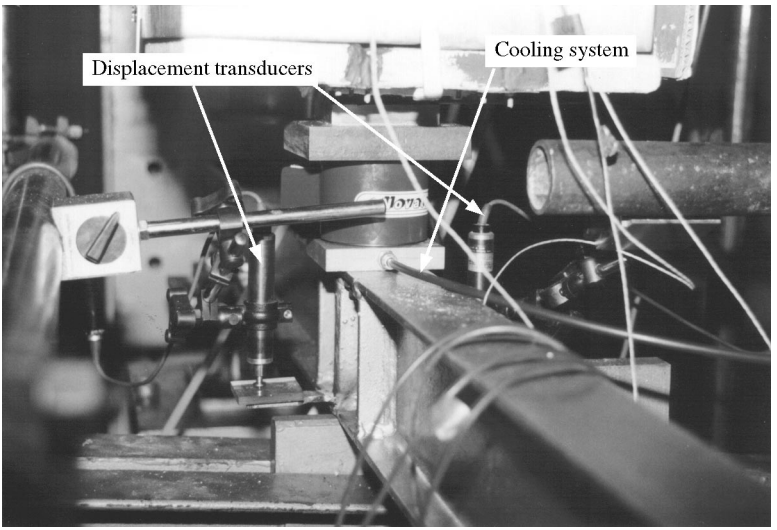

Fig. 7. Measurement of displacements of the lower flange of the stiffness-beam.

attention was drawn to unwanted eventual gaps and to the area of contact surfaces for load transmission that could make the real model deviate from the theoretical one.

3. Test plan

The initial compression load P_0 was chosen as

$$P_0 = 0{,}7 \times N_{\mathrm{Rd,fi},t=0}, \tag{2}$$

where $N_{\mathrm{Rd,fi},t=0}$ is the design value of the buckling resistance of the bar in fire situation at time $t = 0$, that is, the design value of the buckling resistance at room temperature, taking the partial safety factor for the material properties $\gamma_{\mathrm{M,fi}} = 1.0$ [6].

Buckling tests at room temperature were done (Table 1), from which the curves *Axial load — Axial displacement*, characteristic of each bar at room temperature, were obtained. From these curves the maximum compression load $\bar{P}_{\max}$ (mean value) for each pair (eccentricity, slenderness) was obtained, and the real initial load level of each heated bar $P_0/\bar{P}_{\max}$ was calculated (Table 2).

The evolution of the restraining forces is influenced by the stiffness of the cold structure that restrains the elongation and by the shape of the curve *Axial load — Axial displacement* that is characteristic for each heated bar. The shape of this curve depends on the eccentricity e of the compression load and on the slenderness λ of the bar. Thus, the test plan included three tests at high temperature for each combination of these parameters: six values for the stiffness K of the stiffness-beam, four values for the slenderness λ, centred load ($e = 1$ mm) and eccentric load ($e = a$) (Table 2).

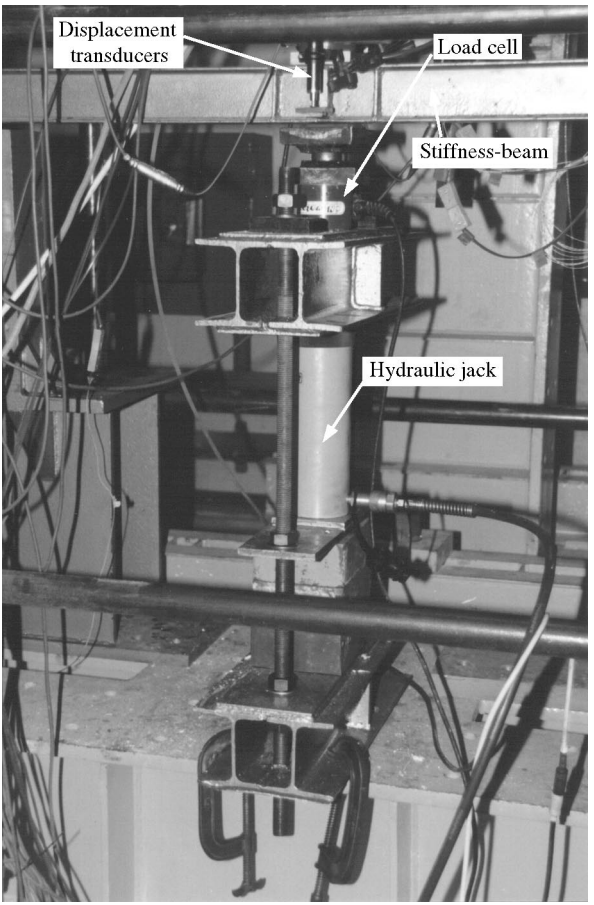

Fig. 8. System for load application.

Table 1
Buckling tests at room temperature

Bar thickness a (mm)	5	8	12	20	5	8	12	20
Load eccentricity e (mm)	1	1	1	1	5	8	12	20
Slenderness λ	319	199	133	80	319	199	133	80
Number of tests	3	3	3	3	3	3	3	3
$\bar{P}_{max}$ (kN)	5.12	19.1	61.04	206.38	4.18	11.28	23.86	52.34

The mean heating rate used in the tests was sufficiently small to allow for convenient temperature homogenisation inside the specimens cross-section. Yet, not so small that it could result in inconvenient over-heating of the load cell located below the lower support of the heated bar. A constant heating rate of 5°C/min was chosen for all tests.

Table 2
Tests at high temperature

Bar thickness a (mm)	5	8	12	20	5	8	12	20
Load eccentricity e (mm)	1	1	1	1	5	8	12	20
Slenderness λ	319	199	133	80	319	199	133	80
P_0 (kN)	2.36	8.88	26.21	84.37	1.48	4.47	10.47	25.03
$P_0/\bar{P}_{max}$	0.46	0.46	0.43	0.41	0.35	0.40	0.44	0.48
Stiffness K (kN/mm)	0, 1, 10, 24, 42, 98							
Number of tests	3 tests each (a, e, K)							

Table 3 shows the values of the yield stress and the ultimate strength of the steel of each bar used to manufacture the test specimens. These values were used in later numerical simulations of the tests. A systematic determination of the Young modulus of the steel was not done. The measured values of this steel property in some of the bars showed a small scatter, between 207.8 and 213.5 GPa. Numerical simulations of the tests showed that changes in the Young modulus within this range had no practical influence on the results.

4. Test results

4.1. Evolution of the temperatures

The temperature evolution in the three zones of the oven (zone 1 — top; zone 2 — middle; zone 3 — bottom) shown in Fig. 9 is characteristic for all the tests and confirms temperature homogeneity inside the oven. These temperatures were

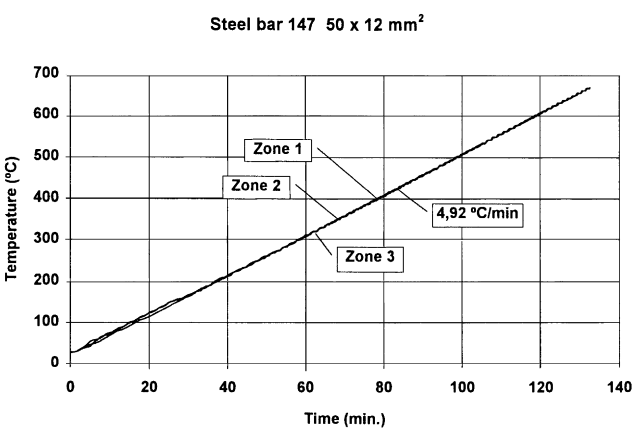

Fig. 9. Temperature evolution inside the oven.

Table 3
Yield stress and ultimate strength of the steel used to manufacture the test specimens

Bar no.	Ultimate strength (MPa)	Yield stress (MPa)
166	444.4	327.5
48	443.5	319.7
86	441.8	324.8
100	446.0	319.9
135	441.8	324.8
158	444.4	327.5
173	444.4	327.5
61	443.5	319.7
77	441.8	324.8
109	446.0	319.9
126	446.0	319.9
186	444.4	327.5
148	450.6	322.7
50	442.7	314.4
88	445.8	318.6
98	450.6	322.7
140	450.6	322.7
150	441.7	317.9
175	441.7	317.9
66	442.7	314.4
75	445.8	318.6
113	445.8	318.6
122	450.6	322.7
183	441.7	317.9
145	428.0	298.9
53	486.8	313.3
93	426.1	290.8
96	426.1	290.8
143	428.0	298.9
154	425.2	291.4
177	425.2	291.4
67	486.8	313.3
71	428.8	292.7
117	426.1	290.8
119	428.0	298.9
181	425.2	291.4

measured near the internal oven surface by the oven thermocouples. The real heating rate was about 4.9°C/min for a programmed value of 5°C/min.

Despite of temperature homogeneity inside the oven, there were temperature gradients along the axis of the heated bars due to heat loss per conduction through the extremities (Figs. 10 and 11).

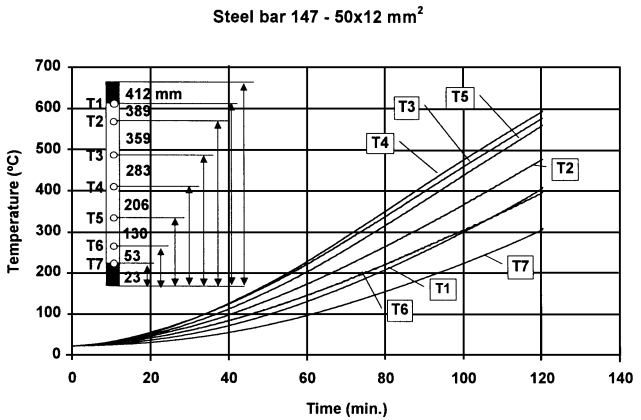

Fig. 10. Temperature evolution at several points of the bar axis.

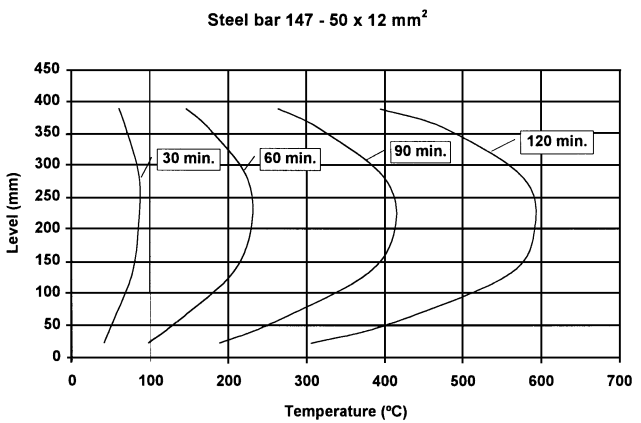

Fig. 11. Temperature gradients along the bar axis.

4.2. Evolution of the restraining forces

For each set of parameters three tests were carried out. The curves shown in Fig. 12 represent the evolution of the restraining forces as a function of the mean temperature of the bar, in three tests for the same set of parameters. The evolution of all the curves is very similar and the scatter is low. The repeatability is quite acceptable. The most important parameter to be measured in the tests was the critical temperature (T_{crit}), that is, the temperature at which the load reaches its initial value again. The maximum difference in the critical mean temperature of the bar in these three tests is about 25°C.

The applied force was controlled by means of a load cell placed between the hydraulic jack and the bottom flange of the stiffness-beam (Fig. 8) and it was kept constant throughout the entire test.

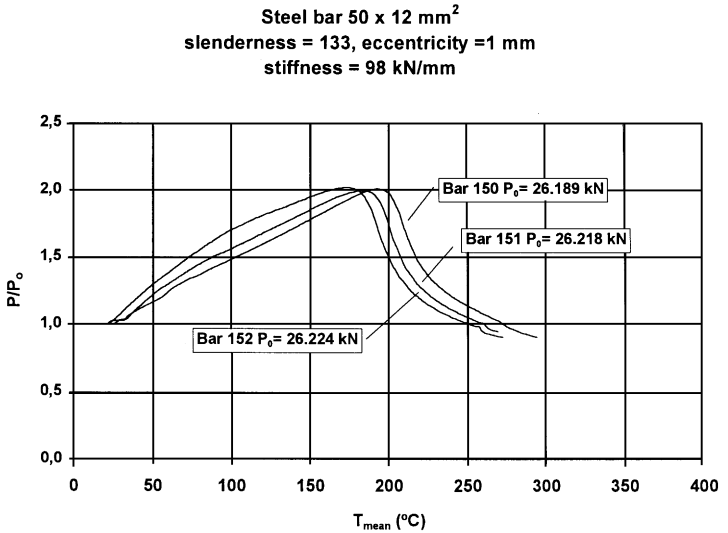

Fig. 12. Evolution of restrained forces in three tests with identical parameters.

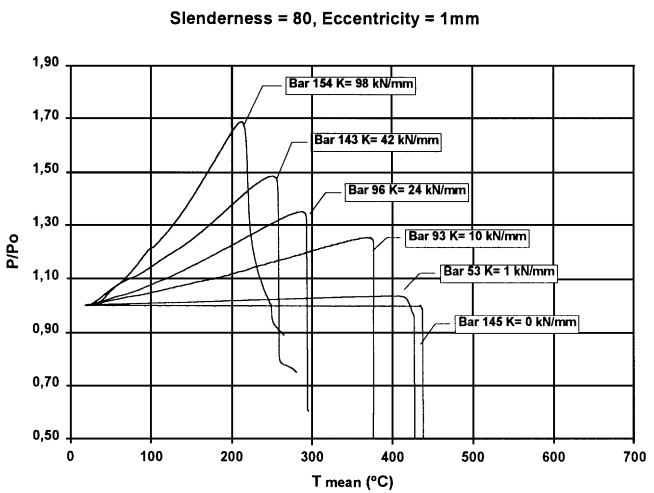

Fig. 13. Evolution of restrained forces — centred load.

Figs. 13–18 show the evolution of the restraining forces as a function of the mean temperature of the bar, for the bar slenderness values of 80, 133 and 199, with centred and eccentric loading, and several stiffness values of the stiffness-beam, ranging from 0 to 98 kN/mm. The mean temperature of the bar was calculated on the basis of the temperature values measured by the seven thermocouples located along its axis (Fig. 10) and the temperatures of two extra thermocouples placed inside the support

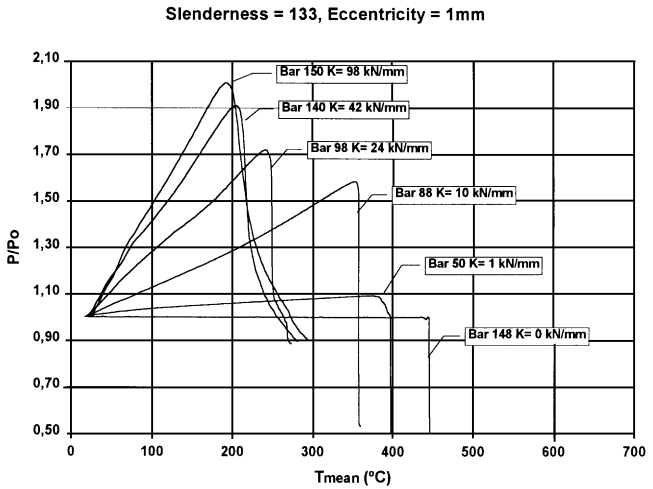

Fig. 14. Evolution of restrained forces — centred load.

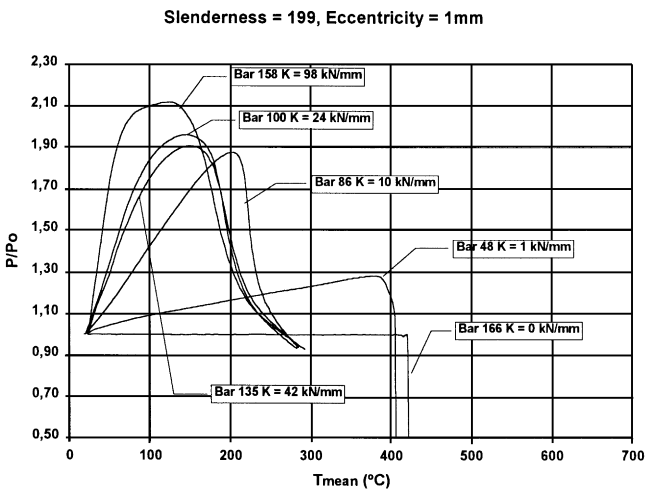

Fig. 15. Evolution of restrained forces — centred load.

cylinders. The stiffness of the stiffness-beam is defined as the vertical load to be applied to the beam to produce a unit vertical displacement. The restraining forces are referred to the initial value P_0, thus resulting in a non-dimensional representation.

The evolution of the deflections of the heated bars during the tests depended upon the value of the load eccentricity and on the stiffness of the stiffness-beam. The bars with eccentric loading deflected continuously from the beginning till the end of the test (Figs. 16–18), showing no sudden changes in the level of the measured restraint load. The bars with centred loading and flexible stiffness-beams showed practically no

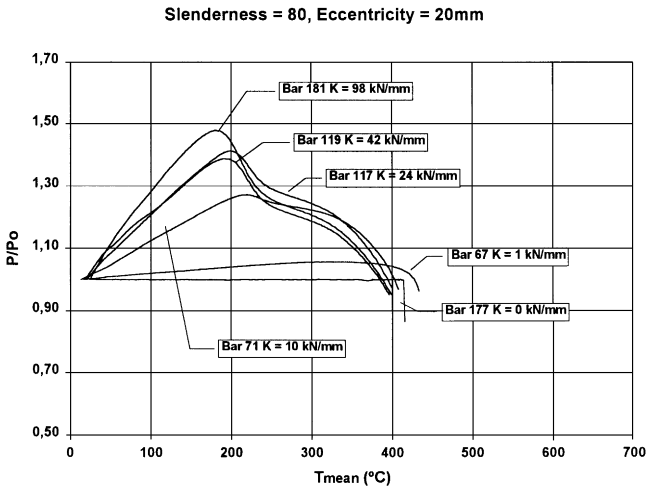

Fig. 16. Evolution of restrained forces — eccentric load.

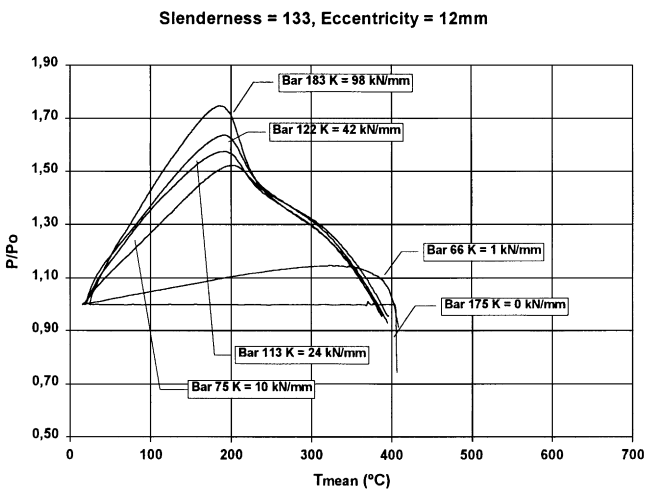

Fig. 17. Evolution of restrained forces — eccentric load.

deflections until the maximum load level was reached and then buckled (Fig. 13 — bars 145, 53, 93, 96, 143; Fig. 14 — bars 148, 50, 88; Fig. 15 — bars 166, 48). When the stiffness of the stiffness-beam was further increased (Fig. 13 — bar 154; Fig. 14 — bars 98, 140) this buckling behaviour was also present, but after a certain sudden reduction in the load level, the deflection rate decreased significantly, followed by a gradual decrease in the restraining forces, until the initial load level was reached. Finally, the bars with centred loading and very rigid stiffness-beams (Fig. 14 — bar 150; Fig. 15 — bars 86, 135, 100, 158) showed no classical buckling behaviour. The drop in the

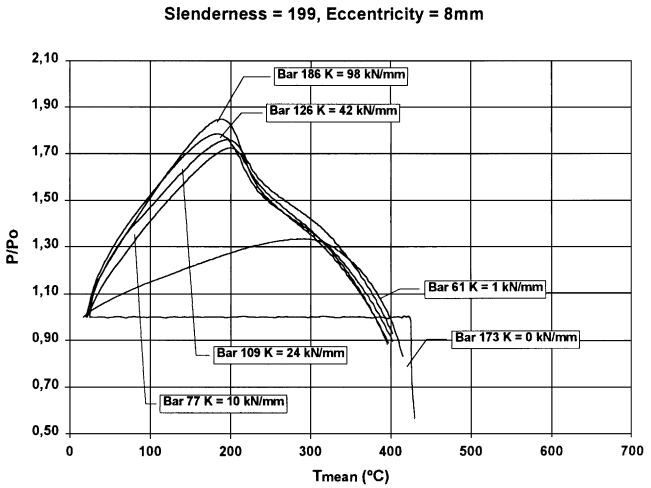

Fig. 18. Evolution of restrained forces — eccentric load.

restraining forces was accompanied by a gradual continuous increase in the deflections.

These results show that neglecting the resistance of columns after the point where the maximum restraint load has been reached, like some simplified methods do, can lead to unnecessary low critical temperatures when the structural stiffness is high. In real structures this stiffness can range from almost zero in one-storey buildings, to very high values for columns in the lower storeys of higher buildings.

For the bars with slenderness 80 and small eccentricity of the load, increasing the stiffness of stiffness-beam causes the curves to intersect the axis $P/P_0 = 1$ at values of the bar's mean temperature which are successively smaller (Fig. 13). The same is observed for the bars with slenderness 133. However, for the higher values of the stiffness, a tendency to stabilization is already visible (Fig. 14). For the bars with slenderness 199 (Fig. 15) it is clearly visible that beyond certain values of the stiffness, the critical temperature undergoes no further decrease, just like numerical simulations earlier concluded for real H sections [8–11]. It should be noted that, for every slenderness ratio, the critical temperature of the bars with centred load diminishes from about 500°C (bar with free elongation) down to about 300°C ($K = 98$ kN/mm). Restraining the thermal elongation of elements with centred load can then cause a decrease in the critical temperature of nearly 200°C.

In the case of eccentric loading, an initial tendency for a very slight decrease in the critical temperature is also observed when the stiffness of the stiffness-beam begins to be increased. In spite of that, it can be said that in general the critical temperature of the bar is not influenced by the value of the stiffness (Figs. 16–18), which also confirms earlier calculation results for real H sections [8–11]. The critical temperature of

Table 4
Critical temperatures

Bar no.	Cross-section (mm)	Eccentricity (mm)	Stiffness (kN/mm)	T_{mean}^{crit} (°C)	T_{max}^{crit} (°C)
166			0	421	578
48			1	405	546
86		1	10	271	387
100			24	262	376
135			42	270	382
158			98	267	382
173	50×8		0	426	574
61			1	402	548
77		8	10	384	529
109			24	396	538
126			42	390	528
186			98	383	523
148			0	446	600
50			1	398	539
88		1	10	359	492
98			24	266	379
140			42	258	364
150			98	274	385
175	50×12		0	406	552
66			1	405	545
75		12	10	389	530
113			24	383	528
122			42	384	527
183			98	385	524
145			0	438	582
53			1	425	569
93		1	10	378	509
96			24	295	408
143			42	261	357
154	50×20		98	251	343
177			0	415	549
67			1	430	570
71		20	10	406	538
117			24	398	532
119			42	388	520
181			98	391	522

elements with sufficiently high eccentricity of the compression load is not influenced much by the restraint to their thermal elongation.

A summary of the critical temperatures obtained in the tests, both in terms of the mean steel temperature of the bars T_{mean}^{crit} and in terms of the maximum temperature in the bar T_{max}^{crit} can be found in Table 4. The stiffness K can be related to the axial stiffness of the heated bars and put into the non-dimensional form KL/EA (Table 5).

Table 5
Non-dimensional stiffness values

K (kN/mm)	A (mm^2)	λ	KL/EA
	50×20	80	0.216
98	50×12	133	0.360
	50×8	199	0.539
	50×20	80	0.092
42	50×12	133	0.154
	50×8	199	0.231
	50×20	80	0.053
24	50×12	133	0.088
	50×8	199	0.132
	50×20	80	0.022
10	50×12	133	0.037
	50×8	199	0.055
	50×20	80	0.002
1	50×12	133	0.004
	50×8	199	0.006

5. Numerical simulations

Numerical simulations of the tests were done using the finite element program FINEFIRE [10].

5.1. Program description

In order to study the behaviour of plane steel structures in fire environment an isoparametric Euler–Bernoulli beam finite element was developed, taking into account geometrical non-linearity by using an approximate up-dated Lagrangian formulation.

The temperature distribution in structures submitted to fire is, in reality, non-homogeneous. So, if this is to be taken into account, different mechanical and thermal material properties must be considered at each point. Numerical Gauss integration points were used to introduce these conditions into the stiffness matrix. In the present simulation the temperature gradients along the bar axis were considered.

For each temperature field and using the Newton–Raphson method, the equilibrium of the structure is obtained by solving the following non-linear equation in order to the displacement field $\{\Delta u\}$:

$$[K(\sigma)]\{\Delta u\} = \{\Delta P\}. \tag{3}$$

The stiffness matrix $[K]$ of the structure is a function of the mechanical properties and of the stress field, and it is updated at each iteration step. The out-of-balance forces are taken into account as applied forces $\{\Delta P\}$ in the next iteration. The equilibrium criterion is based on the out-of-balance forces.

The temperature-dependent constitutive laws and thermal expansion of steel, recommended in Eurocode 3, were used.

5.2. Results

In Figs. 19–24 comparison between test results and calculation results is made for three slenderness values, three stiffness values and centred and eccentric load.

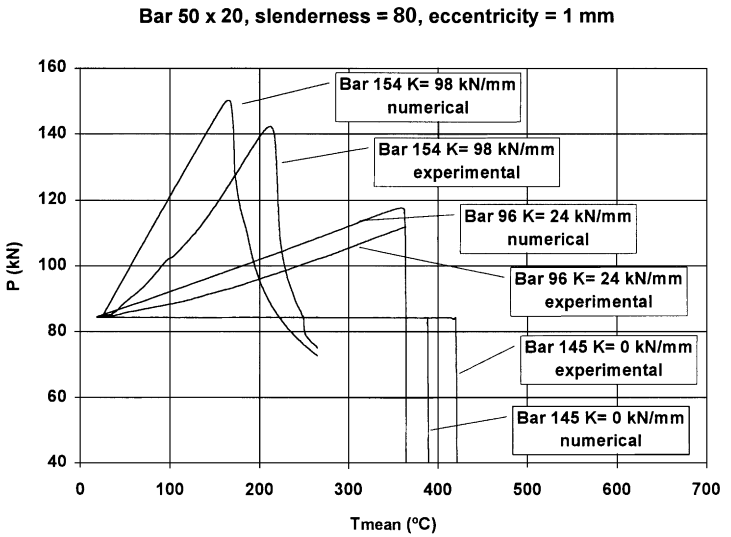

Fig. 19. Numerical simulation — experimental results, centred load.

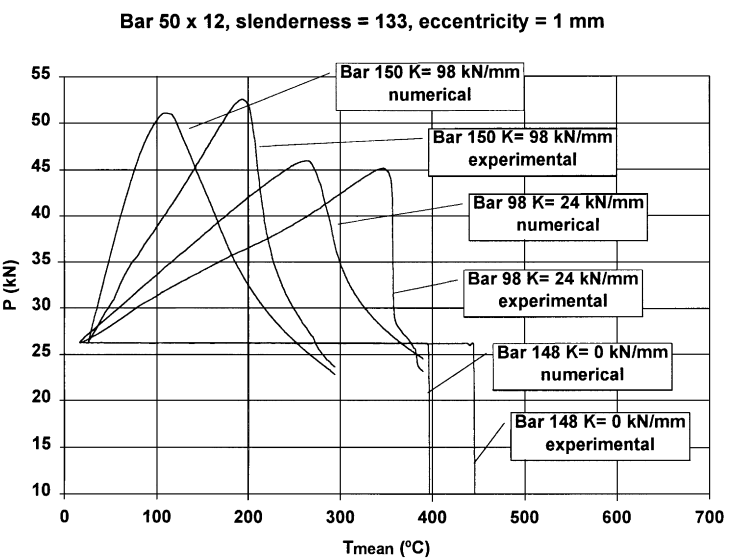

Fig. 20. Numerical simulation — experimental results, centred load.

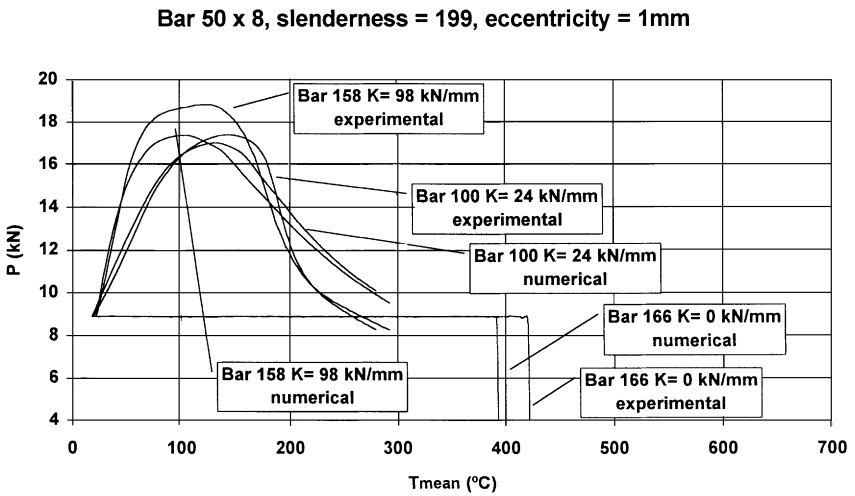

Fig. 21. Numerical simulation — experimental results, centred load.

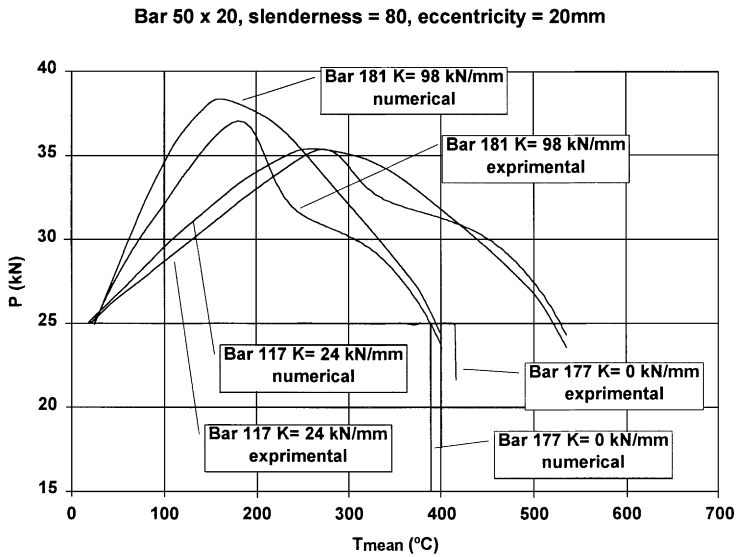

Fig. 22. Numerical simulation — experimental results, eccentric load.

Agreement is acceptable, if consideration is taken of the parameters which are capable of deviating in the assumptions made in the calculations from the real test conditions. One of those factors is friction at the supports. Measures to reduce it were taken but some influence on test results cannot be excluded.

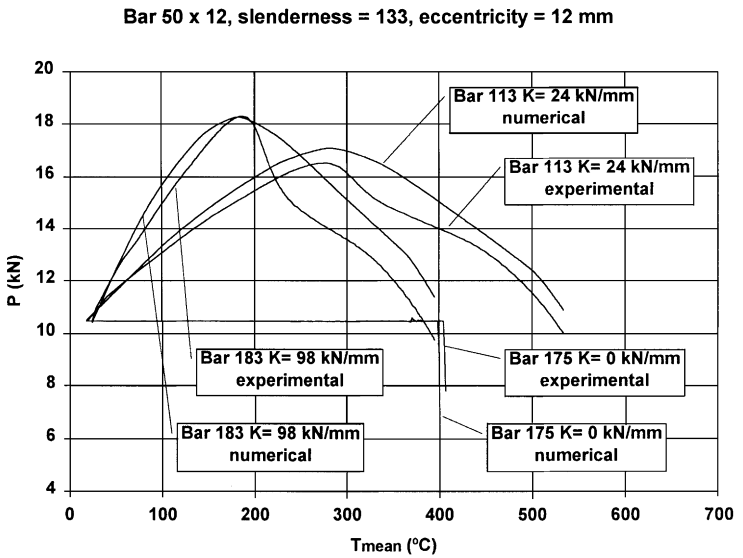

Fig. 23. Numerical simulation — experimental results, eccentric load.

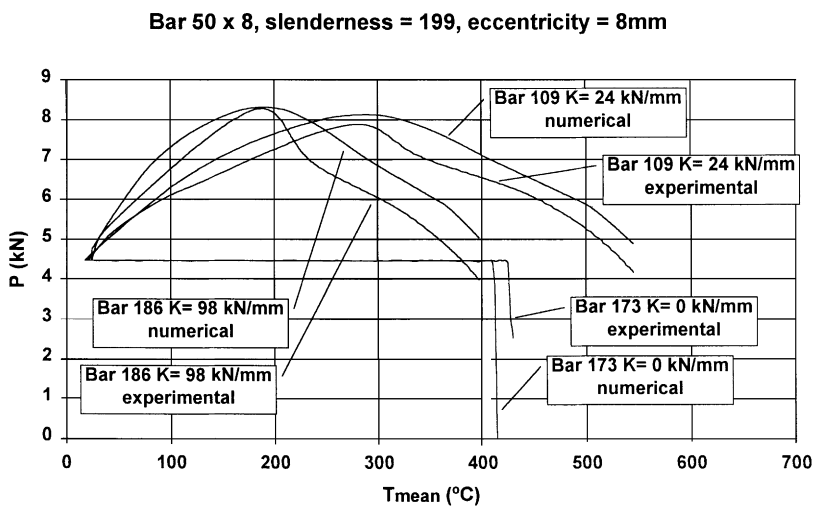

Fig. 24. Numerical simulation — experimental results, eccentric load.

6. Conclusions

A large number of tests on compressed steel hinged elements with thermal elongation elastically restrained were carried out. For each set of test parameters the results obtained showed small scatter. It was observed that the restraint to the thermal

elongation of centrally compressed elements having slenderness higher than 80, can lead to reductions in their critical temperature by up to 200°C. Nevertheless, if the loading is eccentric and the eccentricity is high, the restraint to the elongation does not cause significant variation in the critical temperature. To a great extent, the experimental results confirm the conclusions obtained in earlier calculations with HEB columns [8].

Our major concern should be the fire resistance of the global structure as a whole. Therefore, there might be a reason to treat the fire action differently somehow. If it can be proved that the collapse of a given structural member does not produce the collapse of the rest of the structure or in any way endangers the life of occupants or the correct fire performance of other construction components, then it would be a waste to neglect the residual mechanical resistance of that member after the point when its axial force has decreased to the level of the design effect of actions in fire situation at time $t = 0$. After that point there will be load transfer from the heated column to the cold surrounding elements. This load transfer can be accepted as long as these elements are capable of supporting it without producing the collapse of the structure. This is what happened in the fire Cardington tests [13], where in spite of the squashing of one heated column, no global structural collapse occurred. In most real hyper-static structures this is also what will happen.

In a greater or smaller extent, thermal restraint affects the behaviour of all kinds of structural elements during a fire [14]. However, for columns playing a capital role within the structure, the consideration of thermal restraint may become decisive. Without further testing on steel profiles at real scale the results of this work cannot be directly applicable to common practice, but they show that thermal restraint is something that should be considered.

References

[1] International Standards Organisation: ISO 834. Fire resistance test. Elements of building construction, 1975.
[2] Comité Européen de Normalisation (CEN/TC250/SC1). Eurocode 1: basis of design and actions on structures, Part 2.2: Actions on structures exposed to fire. ENV 1991-2-2, 1995.
[3] Comité Européen de Normalisation (CEN/TC250/SC1). Eurocode 1: basis of design and actions on structures; Part 1: basis of design. ENV 1991-1, 1993.
[4] Comité Européen de Normalisation (CEN/TC250/SC2). Eurocode 2: design of concrete structures; Part 1.2: structural fire design. ENV 1992-1-2, November 1995.
[5] Comité Européen de Normalisation (CEN/TC250/SC3). Eurocode 3: design of steel structures; Part 1.2: structural fire design. ENV 1993-1-2, September 1995.
[6] Comité Européen de Normalisation (CEN/TC250/SC3). Eurocode 3: design of steel structures, Part 1.1: general rules and rules for buildings. ENV 1993-1-1, 1992.
[7] Comité Européen de Normalisation (CEN/TC250/SC4). Eurocode 4: design of composite steel and concrete structures; Part 1.2: structural fire design. ENV 1994-1-2, October 1994.
[8] Cabrita Neves I. The critical temperature of steel columns with restrained thermal elongation. Fire Safety J 1995;24(3):211–27.
[9] Cabrita Neves I, Rodrigues JPC. Resistência ao Fogo de Pilares de Aço. I Encontro Nacional de Construção Metálica e Mista, Porto, Novembro de 1997, pp. 543–550.
[10] Valente JC. Simulação do Comportamento das Estruturas Metálicas Sujeitas a Altas Temperaturas. PhD thesis, Instituto Superior Técnico, Lisboa, Julho de 1988.

[11] Valente JC, Cabrita Neves I. Fire resistance of steel columns with elastically restrained axial elongation and bending. J Construct Steel Res 1999;52(3):319–31.
[12] CTICM. Méthode de Prévision par le Calcul du Comportement au Feu des Structures en Acier, Construction Métalique Vol. 3, Puteaux, Septembre, 1982. p. 39–79.
[13] British Steel Swinden Technology Centre. The Behaviour of Multi-Storey Steel Framed Buildings in Fire. Rotherham, UK, 1999.
[14] Rotter JM, Sanad AM, Usmani AS, Gillie M. Structural performance of redundant structures under local fires. Proceedings of the Interflam'99, Edinburgh, Scotland, June–July, 1999. p. 1069–80.